Macromolecular Research, Vol. 23, No. 10, pp 924-936 (2015)
DOI 10.1007/s13233-015-3126-x

www.springer.com/13233
pISSN 1598-5032 eISSN 2092-7673

Tri-Layered Silk Fibroin and Poly-ε-Caprolactone Small Diameter Vascular Grafts Tested *In vitro* and *In vivo*

A Reum Park[1], Young-Hwan Park*[,1], Hyun Jeong Kim[2], Min-Keun Kim[3], Seong-Gon Kim*[,3], HaeYong Kweon[4], and Subhas C. Kundu[5]

[1]Department of Biosystems & Biomaterials Science and Engineering, Seoul National University, Seoul 151-921, Korea
[2]Department of Dental Anesthesiology and Dental Research Institute, School of Dentistry, Seoul National University, Seoul 110-768, Korea
[3]Department of Oral and Maxillofacial Surgery, Gangneung-Wonju National University, Gangneung, Gangwon 210-702, Korea
[4]Sericultural and Apicultural Materials Division, National Academy of Agricultural Science, Jeonju, Jeonbuk 560-500, Korea
[5]Department of Biotechnology, Indian Institute of Technology Kharagpur (IIT), West Bengal-721302, India

Received May 6, 2015; Revised July 16, 2015; Accepted July 24, 2015

Abstract: A silk fibroin (SF) and poly-ε-caprolactone (PCL) tri-layered nano-fibrous scaffold composed of an inner, middle, and outer layer is fabricated *via* sequential electrospinning. The middle layer of the SF/PCL blend nano-fiber is introduced to minimize delamination of each layer of the scaffold. The inner layer is composed of SF with Spirulina maxima extract (SP), and the outer is composed of PCL. The anti-thrombic effects of SP are tested first. The structure, mechanical properties, and cytocompatibility of the scaffold are evaluated. The tri-layered nano-fiber scaffold is implanted into a rat carotid artery, and the sample after 3 weeks of implantation is evaluated histologically. The SP exerts anti-thrombic activity, and the SF with SP inhibits platelet adhesion. The tri-layered scaffold with the middle layer composed of SF/PCL blend exhibits excellent tensile strengths, burst pressure strength, and suture retention strength. The fabricated material does not induce any cytotoxicity. The cells are well spread on the scaffold. Recipient vessel maintains patency 3 weeks after implantation. The inner lumen of the scaffold reveals regenerated endothelial cells. The results indicate that the tri-layered tubular SF/PCL vascular grafts can be used in vascular tissue engineering due to their excellent mechanical properties and good tissue regeneration capability.

Keywords: silk fibroin, poly-ε-caprolactone, nanofiber, tri-layers, scaffold, vascular tissue engineering.

Introduction

Cardiovascular disease is a leading cause of death and is caused by diseased vessels. Replacement therapy using autografts for the damaged vessels is being tested. There are several limitations of autografts, as follows: (1) the difficulty obtaining healthy vessels from the patient, (2) the unavoidable injury to secondary sites when obtaining autografts, and (3) the size discrepancy between the donor vessel and the recipient vessel.[1,2] Synthetic polymers such as expanded poly-tetrafluoroethylene (e-PTFE) or polyethylene terephthalate (PET) are used for the replacement of large diameter vessels (inner diameter ≥ 6 mm)[3] but are not suitable for small diameter vascular applications. The primary causes of failure are thrombosis and intimal hyperplasia.[4,5]

The development of small diameter artificial vessels has emerged as a challenging and interesting issue. For the successful development of vascular grafts, blood vessel constructs should be designed to mimic the structure of natural vessels. Natural vessels are composed of 3 layers, and each layer has unique properties.[6] This type of multi-layered artificial vessel may have similar features. The graft should have similar or better rheological properties than the corresponding vessel. Too strong a graft may lead to discrepancy in the properties compared to the corresponding vessel and may result in vessel rupture after surgery. Biologically, the vessel graft should not induce thrombosis and intimal hyperplasia.[4,5] Additionally, the graft should induce the ingrowth of endothelial cells. Accelerated endothelialization can inhibit thrombosis and increase the patency rate of the graft.[7] Many natural or synthetic polymer-based scaffolds are used for cell culture. Various combinations of materials have been tested for vessel grafts.[8]

The extracellular matrix (ECM)-like structures can be produced *via* electrospinning. Using the electrospinning technique, different types of polymers have been considered for the small vessel grafts. Natural polymers, such as collagen, elastin, and silk, have shown good cytocompatibility. However, they cannot be used

*Corresponding Authors. E-mails: kimsg@gwnu.ac.kr or nfchempf@snu.ac.kr

for vessel grafts without combining with another material due to their poor rheological characteristics compared to natural vessels.[1,9] The combination vessel graft made up of collagen and poly-ε-caprolactone (PCL) exhibits better mechanical strength than collagen only or PCL-only grafts.[8] Multi-layered artificial vessels composed of PCL and PLA exhibit better mechanical properties than single-layered artificial vessel.[10] To prevent thrombosis, the artificial vessels that incorporate heparin have also been developed.[7] Although multi-layered artificial vessels generally exhibit better mechanical performance, separation at the interface of the layers is frequently observed. Multi-layered artificial vessels combined with PCL and PLA also exhibit the separation between the layers.[10]

Silk protein fibroin (SF) and sericin are being used as natural biomaterials for the fabrication of various matrices such as films, 3D scaffolds/sponges, hydrogels, nano-fibers, and blends with natural and/or synthetic materials for different biomedical applications including optical and electronic materials.[11-14] There are two primary types of silk proteins, namely SF and sericin (glue protein), which are usually obtained from two groups of silkworm species, the domestic mulberry and wild non-mulberry species. SF from mulberry silk is used extensively. The SF is hydrophobic and has most of the properties required of any biomaterial.[15]

There have been many published papers regarding small diameter artificial vessels (inner diameter < 6 mm).[16-20] However, most investigations do not report *in vivo* data. Common strategies of vascular tissue engineering are (1) to graft the vascular scaffold only and (2) to graft a cellularized vascular scaffold. The second strategy has been associated with high success rates because coating the lumen of artificial vessels with endothelial cells can prevent acute thrombosis.[21] As *ex-vivo* endothelial cell cultures require extra time and expense, this strategy is inferior to simple scaffold grafting without an *ex vivo* cell culture. An anti-thrombogenic material, *Spirulinas maxima* (SP) extract has been used for various experiments.[22-24] Therefore, if the artificial vessel has a surface that prevents acute thrombosis, the artificial vessel may be successful without *ex vivo* cell culture.

In this study, the tri-layered artificial vessel with a very small diameter (inner diameter; 1.5 mm) is fabricated *via* the combination of SF and PCL. They are constructed as tri-layered nano-fibrous scaffolds (Figure 1). The inner layer is composed of SF nano-fiber with SP extract. As the vascular scaffold contains an anti-thrombic agent, premedication with an anti-thrombic agent is not necessary. The middle layer is a blended nano-fiber composed of SF and PCL. The outer layer is composed only of PCL nano-fiber. Separation of the layers is prevented due to blended material layers. First, the anti-thrombogenic activity of the SP extract and its inhibition of platelet adhesion are tested. Before producing the tri-layered artificial vessel, each layer is independently fabricated. The layers are evaluated based on their morphology, hydrophilicity, and mechanical properties. The cross section morphology of the artificial vessels are examined using the scanning electron microscopy (SEM). The fabricated artificial vessel is tested for cytotoxicity and cell proliferation. This vessel is grafted into the carotid arteries of the rats and its patency and tissue responses are examined.

Experimental

Materials. Anti-thrombogenic factors were extracted from SP solution. SP was purchased from Nature's Family Australia (Nature's Family Australia, Sydney, Australia). The tablet was grinded using an IKA grinder A10 (IKA, Königswinter,

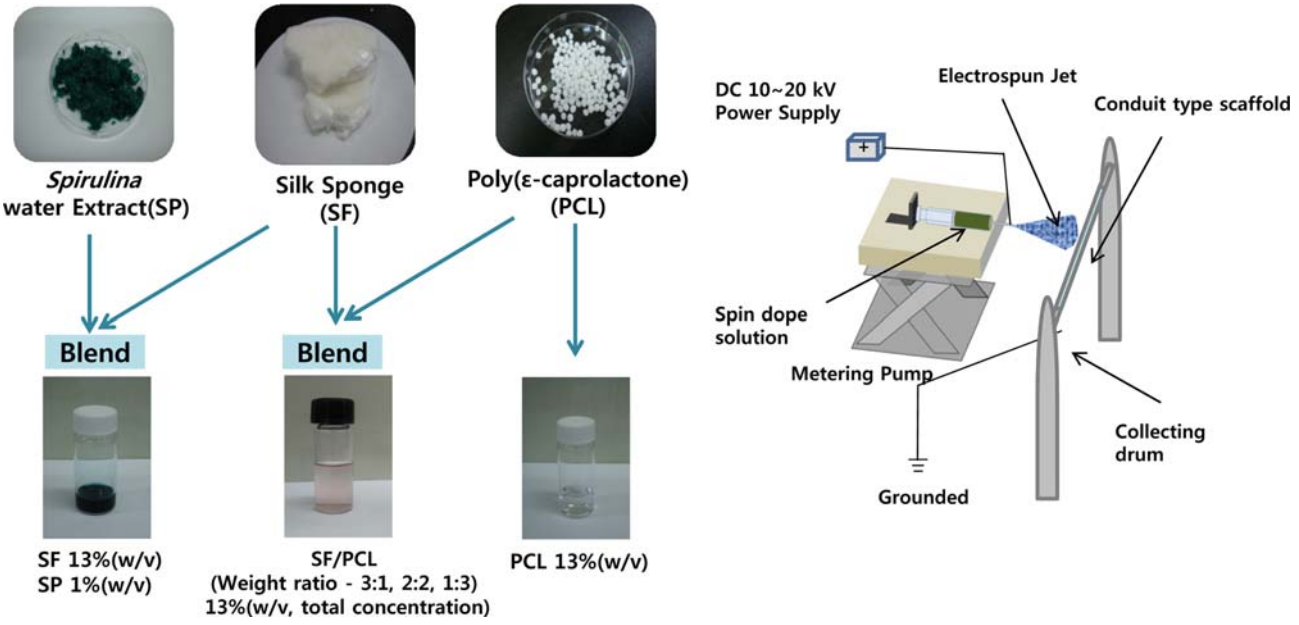

Figure 1. Schematic drawings for the artificial vessel fabrication.

Germany), and a powder was obtained.[25] The powder was solubilized in 1 L distilled water at 4 °C for 24 h followed by centrifugation at 4 °C, 5,000 rpm for 10 min. The supernatant was freeze-dried. This SP extract was used for the following experiments.

Drug Treatment Protocols. Fifteen rats were randomly assigned to intravenous (IV) drug treatment groups corresponding to the vehicle (0.9% saline; 0.5 mL/kg), heparin (375 U/kg), or SP extract (75 mg/kg) to evaluate the efficacy against arterial thrombosis in the rat model. The drugs, freshly dissolved or diluted in 0.9% saline, included heparin sodium (Pharmacia and Upjohn Pty. Ltd, Rydalmere, Australia) and SP extract. This experimental procedures were approved by the Institutional Animal Care and Use Committee of Gangneung-Wonju National University (GWNU 2015-12).

Tail Bleeding Measurements. At the beginning of the experiment, general anesthesia of the animal was induced with 0.2 mL tiletamine and zolazepam (Zoletil 50, Bayer Korea, Seoul, Korea) and 0.1 mL xylazine (Rompun, Bayer Korea, Seoul, Korea). In the anaesthetized rats, a cut was made 3 mm from the tip of the tail to initiate tail bleeding before and at 5 min post-drug administration.[26] The blood was blotted at the end of the cut with tissue paper every 30 s until the bleeding ceased, and the bleeding time (BT) was recorded.

***Ex vivo* Hematological Testing.** In anaesthetized rats (as above), blood (2 mL) was collected from the retroperitoneal vein *via* a puncture 30 min after IV (intravenous) drug administration. To evaluate the efficacy of the SP extract, the collected blood was used at a 9:1 ratio in 3.8% citrate. The samples were transferred to an automated sampler (STAGO, STA Compact), and the activated partial thromboplastin time (aPTT) and prothrombin time (PT) were measured.

Preparation of Regenerated SF. The dried cocoons were degummed by boiling in 0.3% sodium oleate and 0.2% sodium carbonate solution at 100 °C for 1 h. They were then thoroughly washed using distilled water for 4 to 5 times and air dried. The dried fiber was solubilized at 85 °C for 3 min in the solution, which had 1:8:2 molar ratio of $CaCl_2/H_2O/EtOH$. To remove the salt, the solution was dialyzed using cellulose membranes (MW: 12,000-14,000 Da) for 3 days by changing water several times. This solution was freeze-dried as a sponge.

Platelet Adhesion Test. To evaluate the blood compatibility of the SF nano-fibers containing SP extract, we performed both platelet adhesion and plasma protein coagulation tests. Plasma without red and white blood cells of New Zealand white rabbits was obtained *via* centrifuging at 3,000 rpm, and then the platelet rich plasma (1×10^7/mL) was prepared by centrifuging at 5,000 rpm for the platelet adhesion test. The nanofiber scaffold was cut to 5 mm × 5 mm × 0.1 mm and washed with phosphate buffered saline (PBS) before being used for the experiments. The 10 mL of platelet rich plasma was directly seeded on the scaffold, cultured in serum free Dulbecco's Modified Eagle's medium (DMEM) for 1 h and fixed using 10% formalin. The samples were washed three times with PBS, blocked with 1% bovine serum albumin (BSA) in PBS for 30 min at room temperature and incubated for 2 h at 4 °C with Alexa FluorVR 488 Phalloidin (1:250, A12379, Invitrogen™, Carlsbad, CA) for immunofluorescence staining of the cellular structure (F-actin filament) of platelets. After further washing in PBS, the coverslips were mounted with mounting solution (MQ1,Biomeda corp., Foster city, CA) and the samples were analyzed under a confocal microscope (FV-300, Olympus, Japan).

Fabrication of Nano-Fibrous Matrices and Artificial Vessels. The sponge formed SF was used to produce the nanofibrous matrices. PCL (MW: 70,000-90,000 Da) was purchased from Sigma-Aldrich Korea (Gyeonggi, Korea). For electrospinning, 98% formic acid (Kanto chemical, Saitama, Japan) was used as the solvent. The inner layer was produced by electrospinning with 13% (w/v) SF and 1% (w/v) SP extract solution. The outer layer was composed of PCL 13% (w/v). Different mixing ratios (SF:PCL=3:1, 2:2, 1:3) were tested for the middle layer. The solvent mixture was loaded in a 10-mL syringe. The electrospinning conditions were 0.3 mL/h velocity, 12-14 kV voltage, and 20-25 cm spinning distance. The collector was a 90-mm diameter cylinder rotating at 200 rpm. The temperature was set as 25 °C, and the humidity was 40%. A summary of the products are presented in Table I.

The tri-layered artificial vessel was fabricated *via* sequential electrospinning from the inner layer to the outer layer. First, 13% (w/v) SF solution containing 1% (w/v) SP extract was electrospun. Then, the SF/PCL blend solution was electrospun. Three ratios of the blending solutions (SF:PCL=3:1, 2:2, and 1:3 named Triple31, Triple22, and Triple13, respectively) were tested. Then, the 13 % (w/v) PCL solution was electrospun. The thickness of each layer was approximately 70 μm. The overall thickness of the artificial vessel was approximately 200 μm. To fabricate the tubular scaffold, a wire with 1.5 mm diameter was used as the collector. The electrospinning conditions were the same used for the nano-fibrous matrix. The fabricated scaffold was cut to 20 mm in length, washed several times with distilled water, and dried at room temperature.

According to the three blending ratios of the middle layer, three different types of scaffolds were prepared. For com-

Table I. Sample Identification of Electrospun Nano-Fiber Mats[a]

Sample ID	Composition
SFSP	Silk Fibroin 13% (w/v) + *Spirulina* extract 1% (w/v)
SF	Silk Fibroin 13% (w/v)
SFPCL31	Silk Fibroin / PCL (weight ratio 3:1) 13% (w/v, total concentration)
SFPCL22	Silk Fibroin / PCL (weight ratio 2:2) 13% (w/v, total concentration)
SFPCL13	Silk Fibroin / PCL (weight ratio 1:3) 13% (w/v, total concentration)
PCL	PCL 13% (w/v)

[a]PCL: Poly-ε-caprolactone, w/v: weight/volume.

Table II. Sample Identification of Tubular Type Electrospun Nano-Fiber Scaffolds[a]

Sample ID	No. of Layers	Composition		
		Inner Layer	Middle Layer	Outer Layer
Triple31	3	SF 13 % (w/v) + SP 1 % (w/v)	SF/PCL (weight ratio 3:1) 13 % (w/v, total concentration)	PCL 13% (w/v)
Triple22	3	SF 13% (w/v) + SP 1% (w/v)	SF/PCL(weight ratio 2:2) 13 % (w/v, total concentration)	PCL 13% (w/v)
Triple13	3	SF 13 % (w/v) + SP 1 % (w/v)	SF/PCL (weight ratio 1:3) 13 % (w/v, total concentration)	PCL 13% (w/v)
Double	2	SF 13 % (w/v) + SP 1 % (w/v)	-	PCL 13% (w/v)
SFSP*	1	SF 13 % (w/v) + SP 1% (w/v)		
PCL*	1	PCL 13 % (w/v)		

[a]SF: Silk fibroin, SP: *Spirulinas maxima* extract, PCL: Poly-ε-caprolactone, w/v: weight/volume, Triple: tri-layer scaffold, Double: bi-layer scaffold, SFSP*: mono-layer scaffold of SFSP, PCL*: mono-layer scaffold of PCL.

parison, 2-layered scaffolds that did not have a middle layer and mono-layered scaffolds composed of only SF or PCL were also fabricated. A summary of each specimen is presented in Table II.

Morphological Phenotypes and FTIR. The produced fibrous matrices and the artificial vessels were coated with platinum and examined using FE (field emission)-SEM (Supra 55VP, Carl Zeiss, Oberkochen, Germany). The incorporation of SP into the scaffolds was verified using fluorescence microscopy (BX51, Olympus, Japan) based on the exposure of auto-fluorescent material. The duration for light microscopy was set to 5 ms, and the duration for fluorescence microscopy 50 ms.

The chemical structure of the matrix was examined using an FTIR (Fourier transform infrared) spectrometer (ATR FTIR, Nicolet iS5, Thermo Scientific, USA). The specimen had an even thickness (80 μm), and 32 scans were performed. For the heat analysis, 5 mg of each sample were prepared. Under nitrogen gas, the temperature was elevated from room temperature to 350 °C at 10 °C/min using a dynamic scanning calorimeter (DSC) (DSC-Q1000, TA Instrument, New Castle DE USA). The hydrophilicity was analyzed *via* contact angle measurement (Easy drop-Rahmen, Kruss, Germany). Each specimen was prepared at 15 mm×15 mm, and the measurement was repeated 5 times.

Tensile Strength. Using a GS/LRX plus materials testing machine (Lloyd Instruments, Hampshire, UK), the tensional stress, stress-to-strain ratio, and Young's modulus were measured. The measurements were carried out in both dry and wet conditions. The size of the sample was 10 mm×40 mm, and the thickness was 80-100 μm. The gauge length was 20 mm, and the tension speed was 10 mm/min (n=5). Wet conditions were generated by dipping the specimen in distilled water.

To assess whether the scaffold exhibited the proper properties of an artificial vessel, the longitudinal tensile strength and the circumferential tensile strength were measured under the wet conditions. Using a 500-N load cell, each value was measured using a GS/LRX plus materials testing machine (Lloyd Instruments, Hampshire, UK) (n=5).

To measure the longitudinal tensile strength, each specimen was 20 mm in length and 150-200 μm thick. The gauge length was 10 mm, and the tension speed was 10 mm/min. To measure the circumferential tensile strength, previous reports were considered.[27] The length of the specimen was 3 mm. The specimen was fixed to the clamp, the tension speed was set to 0.6 mm/min, and the gauge length was set to the specimen diameter. The maximum stress was set to the ultimate circumferential tensile strength (UCTS). The burst pressure strength of the specimen was calculated based on the UCTS according to Laplace's law.[9,28]

$$\text{Burst pressure (mmHg)} = (\text{UCTS} \times d)/R_0$$

(d: the thickness of the scaffold, R_0: The inner radius of the scaffold under atmospheric pressure, UCTS: ultimate circumferential tensile strength)

To measure the suture retention strength, one end of the specimen was fixed with the lower clamp, and the other end was sutured with 5-0 prolene 2 mm from the margin. The suture material was linked to the upper clamp. The applied tension speed was 20 mm/min.

***In vitro* Test.** The amount of released (tissue necrosis factor) TNF-α was assessed using the RAW 264.7 cell line. The specimens were prepared with dimension of 5 mm×5 mm. The cells were seeded at 1×10^4 cells/25 mm^2 on the prepared specimen. The cells were cultured in DMEM including 10% FBS and 1% penicillin/streptomycin at 37 °C and under 5% CO_2. The supernant was collected at 1, 2, and 3 days. The amount of TNF-α was determined using a commercially available mouse TNF-α immunoassay kit. The subsequent procedure was followed as per the manufacture's protocol.

Cell viability was quantified after 48 h of the cell growth using a tetrazolium salt 3-(4,5-dimethylthiazole-2-yl)-2,5-diphenyltetrazolium bromide (MTT) assay. NIH 3T3 mouse fibroblasts and human umbilical vein endothelial cell (HUVEC)

were used. For the TNF-α assay, the specimen was prepared with dimensions of 5 mm×5 mm. The numbers of seeded cells were 2×10^4 cells/25 mm^2 NIH 3T3 mouse fibroblasts and 1×10^4 cells/25 mm^2 HUVEC cells. The culture medium for the NIH 3T3 mouse fibroblasts was the same as that used for the RAW 264.7 cells. For the HUVEC cells, an EGM-2 bullet kit (EBM-2 medium including hEGF, hydrocortisone, GA-1000, FBS, VEGF, hFGF-B, R3-IGF-1, ascorbic acid, and heparin) was used. The cells were cultured for 1, 3, and 5 days. The cells were incubated with MTT solution (Cell proliferation kit I; Roche Molecular Biochemicals, Mannheim, Germany) in six-well plates for 4 h at 37 ºC in an atmosphere of 5% CO_2 and 99% relative humidity. The product was estimated by measuring absorbance at 590 nm using a Victor Multilabel counter (Perkin-Elmer-Wallac, Freiburg, Germany). Additionally, the cells attached to the specimen on 1, 3, and 5 days were fixed in 2.5% glutaraldehyde (Sigma Aldrich, Gyeonggi, Korea) and dehydrated with ethanol. They were then coated with platinum and observed under SEM.

***In vivo* Test.** Two 12-week-old Sprague-Dawley rats weighing 250 to 300 g were obtained from Samtako Bio Korea Co. (Gyeonggi, Korea). Each rat was housed in separate stainless steel cages and allowed to adapt to the conditions of the animal house for 10 days prior to starting the experiment. The animals were maintained on a 12 h dark/light cycle at approximately 22±3 ºC. They were allowed free access to the standard laboratory diet and tap water ad libitum during experiments. This experiment was approved by the Institutional Animal Care and Use Committee of Gangneung-Wonju National University (GWNU 2014-17).

In anaesthetized rats (as above), the right carotid artery of each animal was carefully dissected from the adjacent tissues. Two vessel claps were placed on the carotid artery to prevent blood leakage. The carotid artery was cut using micro-scissors. The resected length of the carotid artery was approximately 2 mm. Each end of the carotid artery was sutured using a 10-0 nylon suture under microscopy to the end of the artificial vessel for re-anastomosis. After micro-suturing, the inner most layer of the artificial vessels was in direct contact with the outer most surface of the carotid artery. After finishing anastomosis, the milking patency test was performed for each animal to evaluate arterial functions. Two pre-sterilized and pre-bended #300 wires for indexing the reconstructed areas for the later Doppler analysis were tagged.

Color Doppler Sonography. On the operation day and 3 weeks post-operation, we used an ultrasonic machine (ACCUVIX V10®, Samsung Medison, Seoul, Korea) to evaluate the function of the re-constructed carotid artery. Post-operative color Doppler sonography of the common carotid artery was performed on each rat to monitor the vessel. The sonography allowed for the determination of acute thrombosis and hemodynamic changes, including peak systolic velocity (PSV), end-diastolic velocity (EDV), pulse index (PI), and resistance index (RI). Prior to the color Doppler sonography evaluation, general anesthesia of the animal was induced with 0.2 mL of tiletamine plus zolazepam (Zoletil 50) and 0.1 mL of xylazine (Rompun). First, the wires were identified, which were tagged the outer sides of both of the micro-suturing areas to confirming the correct reconstructed vessels. We checked blood flows using an ultrasonic probe, which was positioned parallel to the carotid artery.

Angiography. Visipaque® (Amershan Health, Cork, Ireland) was used for the angiographic analysis. The inferior vena cava was dissected and intravenously catheterized using a 24-gauze IV catheter. Visipaque® (0.3 mL) was injected, and X-rays of both carotid arteries were immediately taken. The entire vascular status of constrictions and the vascular diameter was compared with the opposite normal carotid artery in the live rats. After angiography, the animals were sacrificed for histological analyses.

Histological Analysis. After fixation, the vascular grafts were dehydrated in increasing concentrations of alcohol solutions, clarified in xylene, and embedded in paraffin. Five micron embedded samples were cut using a microtome, and the sections were stained using hematoxylin and eosin. The rate of local tolerance was analyzed based on the presence of fibrous tissue, degenerative phenomena, necrosis, neo-vessels, calcification, inflammatory cells, and material degradation of the SF graft. To confirm endothelial cell regeneration, immunohistochemical staining for von Willebrand factor (#sc14014, Santa Cruz Biotechnology, Santa Cruz, CA) was carried out.

Statistical Analysis. Analysis of variance (ANOVA) was used to compare the groups of the cell culture and animal study. For post-hoc tests, Bonferroni's method was used. The significant level was set at $p<0.05$.

Results and Discussion

Anti-Thrombic Activity of SP Extract. The SP extract exhibited anti-thrombic activity (Figure 2) and should be included in the inner layer to prevent thrombus formation. As demonstrated by tail bleeding measurements and the *ex vivo* hematological test, the SP extract inhibited blood clotting at 75 mg/kg concentration (Figure 2(a)-(c)). Correspondingly, BT increased by 2-fold for 75 mg/kg of SP extract (Figure 2(a)). The BT was 3.23±2.05 min, 7.09±1.94 min, and 9.53±2.07 min for the saline, SP extract, and heparin treatments, respectively (p=0.001). The post-hoc test revealed significantly higher values if the SP extract and heparin groups compared with the saline-treated control group (p=0.033 for SP extract and p=0.001 for heparin). There were no significant differences in PT (Figure 2(b), $p>0.05$) among groups. The aPTT was 41.90±8.23 s, 57.63±12.50 s, and 149.60±60.80 s for the saline, SP extract, and heparin treatments, respectively (Figure 2(c), p=0.002). The post-hoc test revealed significantly higher values for the heparin compared saline-treated groups (p=0.003). However, no significant difference between the SP extract-

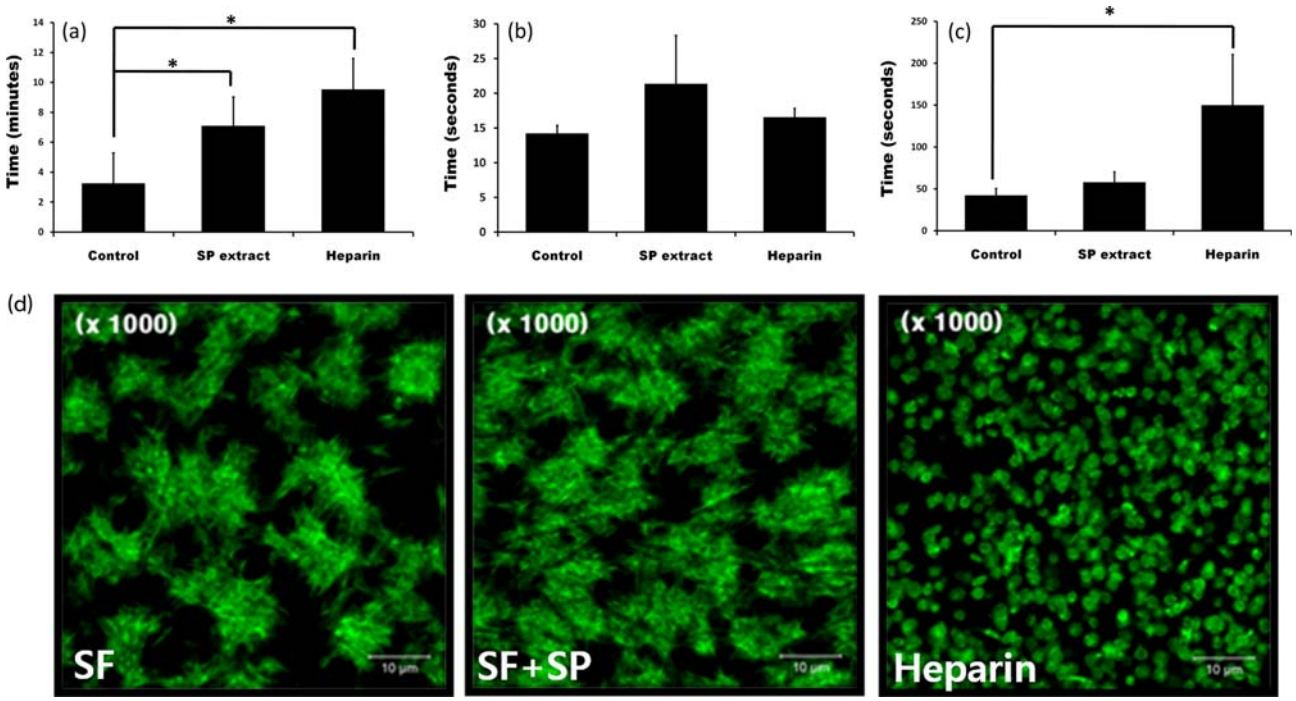

Figure 2. The anti-thrombic assay: (a) Bleeding time (BT) assay, (b) prothrombin (PT) time assay, (c) activated partial thromboplastin time (aPTT), and (d) the confocal fluorescence microscope images of platelet adhesion.

treated group and saline-treated group (p>0.05) was observed. For the SF scaffold with SP extract, the viscosity and electric conductivity increased for increasing contents of SP extract.[24] The low concentration of SP was less influenced by the viscosity, and the electrospun fiber had a small diameter. However, the anti-thrombic activity of SP would be weak for low concentrations of SP.[24] High concentrations of SP induced irregular shapes and large diameter vessels.[29] In this study, the SF scaffold with SP extract (1% w/v) yielded a larger fiber diameter. Although the concentration of SP was not high, adhesion of the platelets was inhibited.

The confocal fluorescence microscope images of platelet adhesion onto the SF nano-fiber containing 1% w/v were observed. The SP extract exhibited less platelet adhesion compared to pure SF nano-fibers. The SF nano-fiber containing 1% (w/v) heparin exhibited the least platelet adhesion among the three groups (Figure 2(d)).

Structure and Morphology of the Fabricated Electrospun Mats. The morphologies of the SF, PCL, and SF/PCL blended matrices are presented in Figure S1. The average diameters of the electrospun nano-fiber are shown in Supplementary Table I. The overall average diameters of the matrices ranged from 200 to 400 nm. Particularly, the SF/PCL blended matrix exhibited higher variations.

The FTIR spectrum of the SP extract is shown in Figure S2(a). The absorbance band near 3300 cm^{-1} was due to the hydrogen bonded -OH and stretching of -NH_2.[30] Peaks due to the presence of protein (amide I peak: 1630-1650 cm^{-1}, amide II peak: 1530-1540 cm^{-1}, amide III peak: 1230-1270 cm^{-1}, and amide V peak: 640-800 cm^{-1}) were also observed. The peaks due to the sulfur oxide were observed at 1040 cm^{-1} and 670 cm^{-1}.[31] The SP extract contained hydrophilic salts and protein. SF with 1% w/v SP extract exhibited a similar spectrum to SF only. The FTIR spectrum of PCL revealed 2949 cm^{-1} and 2865 cm^{-1} peaks due to CH_2 stretching and a 1727 cm^{-1} peak due to C=O stretching.[32] The SF/PCL blended matrix exhibited a mixture of peaks, which were observed in the FTIR spectrum of SF and PCL.

The DSC thermal analysis results of the SF matrix with SP extract and the SF/PCL blended matrix are presented (Figure S2(b)). The SF matrix had a broad heat absorbance band near 40-115 °C and a sharp heat absorbance peak at 280 °C. The heat absorbance transition of the PCL matrix was 57.2 °C. The SF/PCL blended matrix exhibited peaks corresponding to the heat transition of SF and PCL. The heat absorbance peaks were not influenced by the mixing ratio. The height of each peak was dependent on the blending ratios. The contact angle of each fibrous matrix is presented in Table SII. The PCL matrix had a contact angle of 72°, and the SF matrix had a contact angle of 62°. The SF/PCL blend matrix exhibited a decreased contact angle when the SF content was increased. The SF matrix with SP extract had a smaller contact angle compared to SF only.

The stress-strain curves of each dried matrix are shown (Figure S3(a)). The SF matrix exhibited a relatively higher tensile strength and less than 5% strain. SF had a high Young's modulus. SF with 1% w/v SP exhibited similar properties. However, the PCL matrix exhibited high strain and a low

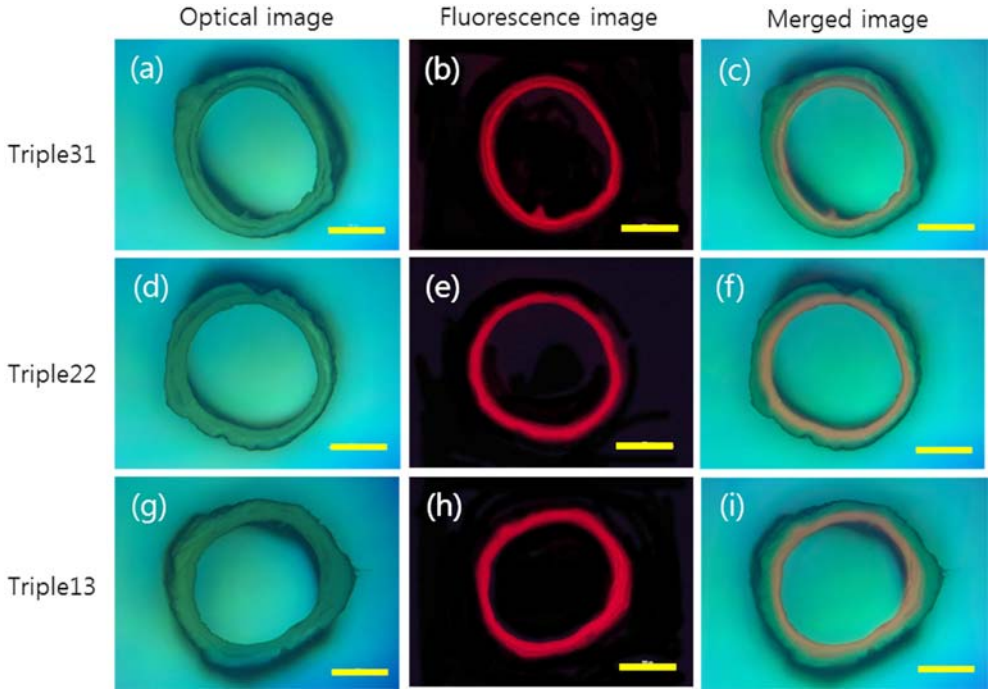

Figure 3. Optical (a, d, g), fluorescence (b, e, h), and merged (c, f, i) images of the cross-sections of tubular type nano-fiber scaffold (×50, scale bar: 500 μm).

Young's modulus. The SF/PCL blended matrix exhibited properties between the SF and PCL matrices. The PCL content of the SF/PCL blended matrix exhibited a higher breaking strain when the PCL content was increased. The maximum tensile strength was independent of the SF/PCL ratio similar to that of the SF matrix.

The stress-strain curve of each matrix under wet conditions are presented in Figure S3(b). Compared to dried conditions, the maximum breaking stress of SF was decreased to 1/4, and Young's modulus was also decreased. The strain was increased 8 times. On the contrary, the PCL matrix exhibited similar value as in the dried state. The SF/PCL blended matrix exhibited different values for the dried and wet states. The tensile strength of the SF/PCL blended matrix in the wet condition was dependent on the PCL content.

Structure and Morphology of the Tubular Scaffolds. The morphology of the nano-fibrous matrix was dependent on its content. The morphology of the artificial vessel is presented in Figure 3. Although the artificial vessel was washed after production, SP was still identified in the scaffold and induced fluorescence (Figure 3). The FE-SEM images of each scaffold were observed (Figure 4). The scaffold without the middle layer exhibited contracture and separation between the inner and outer layers. The scaffold with the middle layer composed of the SF/PCL blended matrix exhibited a stable morphology (Figure 4(b)-(d)) compared to the scaffold without the middle layer (Figure 4(a)). The inter-layer separation was reduced due to introduction of the middle layer. Compared to the 3:1 or 1:3 mixing ratio, the 2:2 SF/PCL blended matrix exhibited less inter-layer separation.

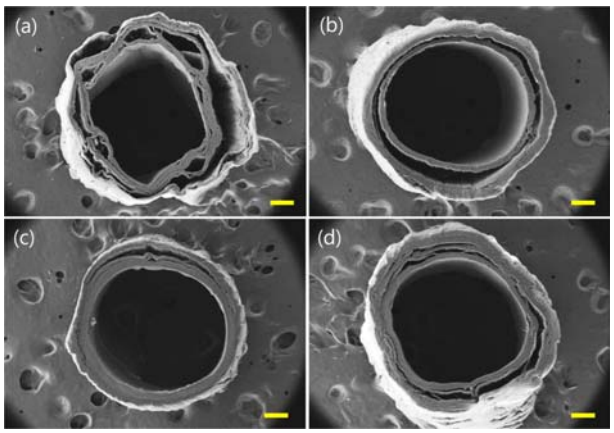

Figure 4. FE-SEM images of the cross-section of tubular type nano-fiber scaffolds (a) double, (b) triple31, (c) triple22, and (d) triple13 (×100, scale bar: 200 μm).

For the electrospinning of the PCL nano-fibers, 14 kV of voltage was applied. High voltages with an acidic solvent (formic acid) may degrade PCL and reduce the viscosity. As a result, the average diameter of the PCL fiber was 179 nm, which is relatively small. The high variation in the fiber diameter of the SF/PCL blend may be due to low compatibility between the two materials. The average diameter was increased as the PCL content was increased. The FTIR analysis revealed that the SF/PCL blended matrix had both SF- and PCL-specific peaks. Regarding the thermal analysis of the SF-only

matrix, the heat absorbance peak approximately 40-115 °C was due to water evaporation, and the peak near 280 °C was due to the breakage of SF chain.[33,34] For the PCL matrix, the peak at 57.2 °C was due to melting PCL.[35] The SF/PCL blended matrix exhibited mixed peaks of SF and PCL. SF is mainly composed of glycine and alanine, which are hydrophobic amino acids. Therefore, the SF is primarily hydrophobic. SF is more hydrophilic than PCL. Accordingly, the SF/PCL blended matrix exhibited a smaller contact angle with increasing SF content. The SF contained SP exhibited a smaller contact angle compared to SF only, which may be due to the proteins and the polysaccharides of SP.[24,25]

Mechanical Properties of the Tubular Scaffolds. The result of the longitudinal tensile strength is presented in Figure S4. Compared to the mono-layered structure, the multi-layered scaffold had more than two peak points. The two-layered scaffold revealed that the inner SF layer broke first, followed by the outer PCL (Figure S4). Compared to the SF-only scaffold, the PCL scaffold exhibited superior longitudinal tensile strength. The tri-layered vessel scaffold showed two steps or three steps of breakage depending on the SF/PCL blending ratio (SF:PCL=3:1, 2:2, and 1:3 named as Triple31, Triple22, and Triple13, respectively). For the Triple31 and Triple13, independent breakage of the middle layer was not observed,

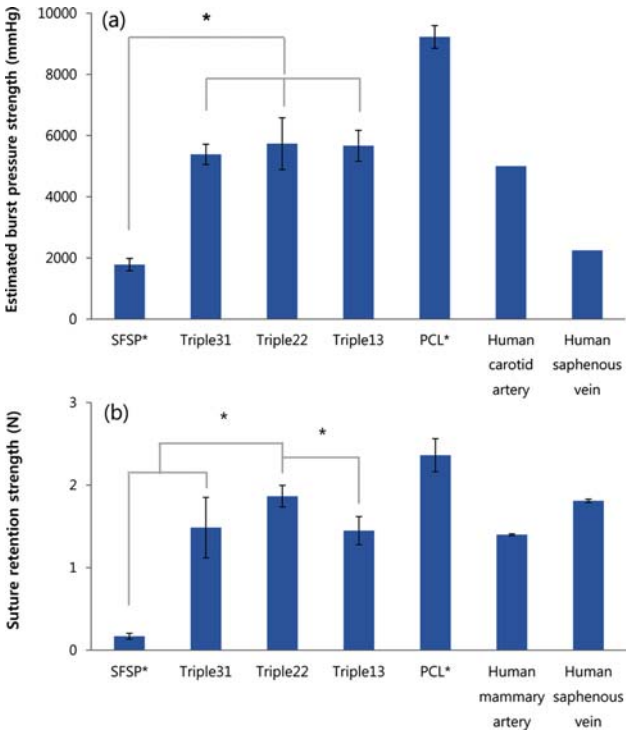

Figure 5. (a) The estimated burst pressure strength of the tubular type nano-fiber scaffold in comparison to that of native blood vessels (*significantly different at $p<0.05$, n=5). (b) Suture retention strength of the tubular type nano-fiber scaffold in comparison to that of native blood vessels (*significantly different at $p<0.05$, n=5).

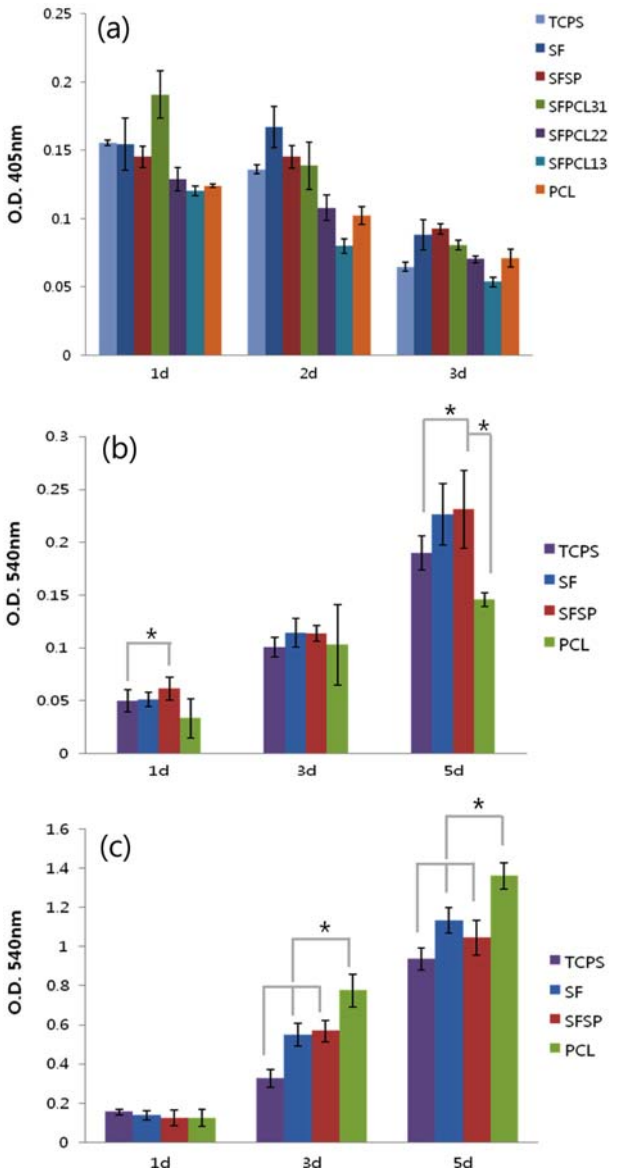

Figure 6. The biological evaluations. (a) TNF-α assay of SFSP, SF, SF/PCL blend, and PCL nano-fiber scaffolds, (b) MTT assay of HUVECs on SF, SFSP, and PCL nano-fiber scaffolds (after 1, 3, 5 days of cell culture, *significantly different at $p<0.05$, n=6), and (c) MTT assay of the fibroblast cells on SF, SFSP, and PCL nano-fiber scaffolds (after 1, 3, 5 days of cell culture, *significantly different at $p<0.05$, n=6).

and two peak points were observed. Triple22 exhibited independent breakage of the middle layer and had three peak points. When the physical properties of tri-layered vessel scaffolds were reviewed (Figure S4), the scaffolds had similar strain and breakage stress compared to the PCL scaffold. Particularly, the Triple22 group had a higher breaking strength and Young's modulus compared to the Triple13 and the Triple31 groups.

The circumferential tensile strengths are shown in Figure S5. The PCL vessel scaffold exhibited a higher circumferential

tensile strength compared to the other scaffolds. The SF scaffold with SP extract showed a lower circumferential tensile strength and strain. Tri-layered scaffold showed similar results regardless of the blending ratio. The SF scaffold exhibited a higher Young's modulus in the wet conditions. Compared to the natural vessel, the tri-layered scaffold exhibited 5300-5700 mmHg of rupture stress, which was lower compared to the PCL scaffold, but much higher compared to the SF scaffold with SP extract.

SF scaffold with SP extract exhibited a lower suture burst stress (Figure 5), and the PCL scaffold had a higher suture burst stress. The tri-layered scaffold showed lower suture burst stress than the PCL-only scaffold, which was 10 times higher than the SF-only scaffold. The suture burst stress of the tri-layered scaffold was 1.44-1.86 N. Among them, the Triple22 showed the highest value.

The artificial vessel should be sutured into the corresponding natural vessel, and therefore, the scaffold should have the proper suture burst stress, which is an important parameter for successfully grafting vessels.[8] The minimum suture burst stress required for artificial vessels is more than 2.0 N.[36] The human mammary artery exerts 1.4±0.01 N of suture burst stress, and the human saphenous vein exerts 1.81±0.02 N.[37] In our study, the suture burst stress of the tri-layered scaffold was 1.44-1.86 N of which the Triple22 exhibited the highest value. Therefore, the Triple22 scaffold was selected for the animal experiments.

The tri-layered scaffold matrix had a similar cutting strain and a higher maximum cutting strength compared to the natural vessel. The human carotid artery has a cutting strength of 0.95±0.13 MPa and a cutting strain of 125±15%. The porcine coronary artery has a cutting strength of 2.6 MPa and a cutting strain of 146±1%.[27,32] Our fabricated tri-layered scaffold exhibited a cutting strength of 6 to 8 MPa and a cutting strain of 135 to 140%. In this study, the tri-layered scaffold exhibited a 5300-5700 mmHg rupture stress, whereas the human carotid artery has a rupture stress of 5000 mmHg and the saphenous vein has a rupture stress of 2250 mmHg.[38] Therefore, the tri-layered scaffold exhibited a comparable rupture stress to natural vessels.

Cell Proliferation and Morphology of HUVECs on the Tubular Scaffolds. The results of the TNF-α assay revealed that there was no significant difference of TNF-α value compared to the untreated control (Figure 6(a)). The MTT results of the HUVECs on the SF scaffold with or without SP exhibited higher values compared to the PCL-only scaffold (Figure 6(b)). The fibroblast on PCL-only scaffold showed higher MTT value than SF scaffold with or without SP (Figure 6(c)).

Differences in the cellular attachment of HUVEC cells were observed from day 1 (Figure 7). The SF scaffold with or without SP revealed flattened HUVEC cells from day 1. However, the PCL-only scaffold revealed spherical shaped

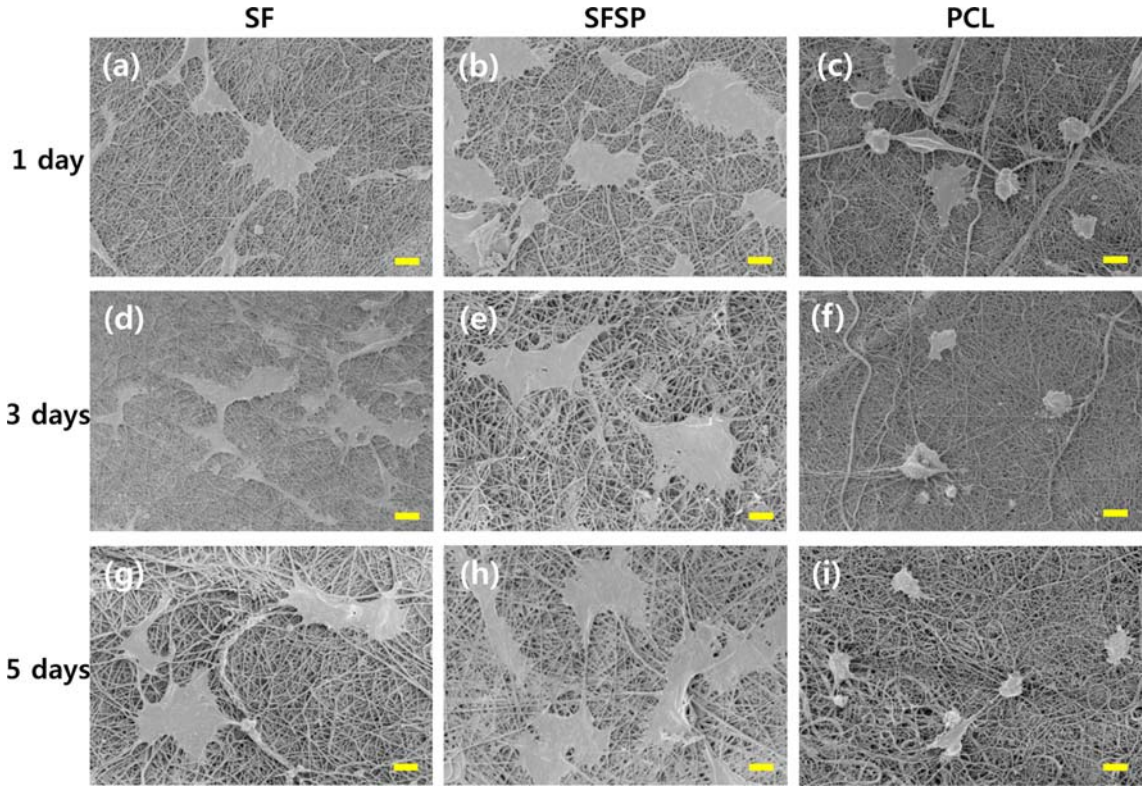

Figure 7. FE-SEM images of HUVECs on SF (a, d, g), SFSP (b, e, h), and PCL (c, f, i) nano-fiber scaffold for 1 (a-c), 3 (d-f), and 5 (g-i) days after cell seeding (×2000, scale bar: 10 μm).

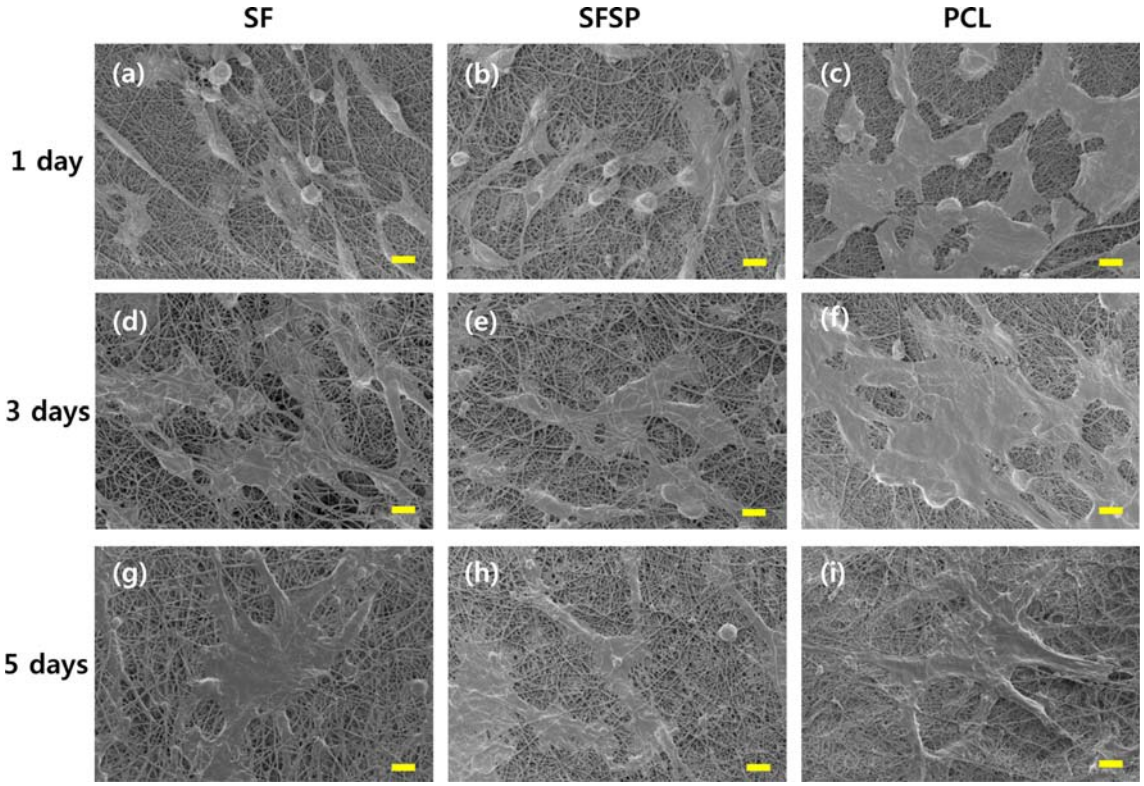

Figure 8. FE-SEM images of fibroblast cells on SF (a, d, g), SFSP (b, e, h), and PCL (c, f, i) nano-fibers for 1 (a-c), 3 (d-f), and 5 (g-i) days after cell seeding (×2000, scale bar: 10 μm).

cells. These trends were observed until day 5. For the PCL-only scaffold, some cells appeared flattened at day 5. Fibroblast exhibited a different trend. The PCL-only scaffold revealed well spreading cells at day 1 (Figure 8). The SF scaffold with or without SP revealed spherical shaped cells.

Natural vessels have three layers. The inner layer is composed of endothelial cells, the middle layer is composed of muscle cells, and the outer layer is composed of primarily fibroblasts.[39] For the results of HUVEC cells, the SF scaffold with or without SP extract exhibited a higher MTT value compared to the PCL-only scaffold. The SF scaffold with SP extract exhibited a similar value to the SF-only scaffold. Thus, SF scaffold with SP extract did not inhibit the proliferation of the endothelial cells. The endothelial cells increase their proliferation when the hydrophilicity of the scaffold is increased.[40] For fibroblasts, the PCL scaffold exhibited a higher MTT value than that of the SF scaffold with or without SP extract. Cellular proliferation is influenced by the chemical composition of the scaffold.[41,42] The inner layer of natural vessels is lined with endothelial cells, and therefore, the inner layer

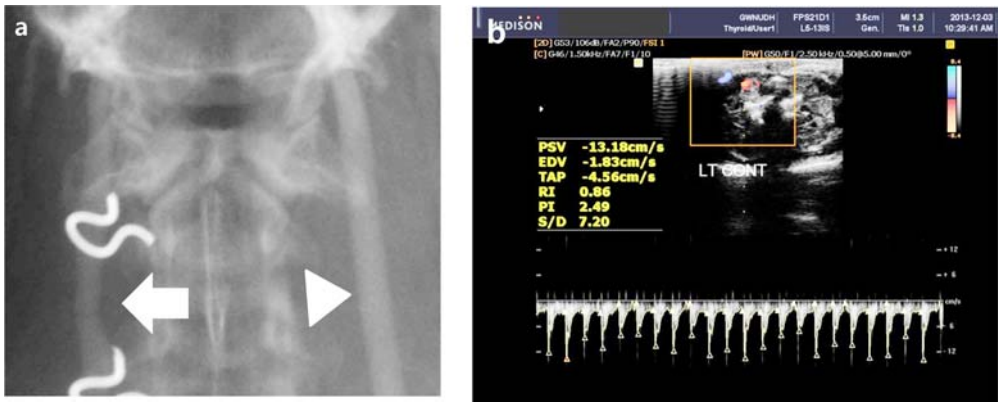

Figure 9. *In vivo* tests. (a) Angiography at 3 weeks after grafting. The grafted vessel (arrow) does function and there is no narrowing, which might be potentially induced by the intimal hyperplasia. In comparision to unoperated counterpart (arrow head), the vessel patency well maintained and (b) color Doppler sonogram also show pulsatile movement.

Table III. Selected Worked Being Carried Out Using Silk Protein/Other Natural Protein Matrices for Vascular Grafts through Electrospinning or Other Techniques in Vascular Tissue Engineering[a]

No.	Materials	Methods	*In vivo* experiment/ Recipient vessel	Inner diameter of vessel	Merits/demerits	Ref.
1	SF/SF, SF/G, PET/ SF, PET/G(Base/ coating material)	Double-raschel knitting	Rat/abdominal aorta	1.5 mm	Large scale animal study/No functional analysis and systemic heparin administration	16
2	SF/SF-H1/SF-H3	Degumming	No	NS	Inner layer has heparin/No animal study	43
3	SF/Type I collagen	Electrospun	No	6 mm	Collagen reinforced/No animal study	44
4	SF/PLGA	γ irradiation	No	NS	Improvement of both hemocompatibility and endothelialization/No animal study	45
5	SF	Double-raschel knitting, degumming	Rat/abdominal aorta	1.5 mm	Good Elasticity, flexibility, inhibition of intimal hyperplasia/ No functional analysis and systemic heparin administration	17
6	SF/ePTFE	Gel spinning	Rat/abdominal aorta	1.0 - 1.5 mm	Biodegradability, vascular cell remodeling, control of material deposition/No functional analysis and systemic heparin administration	18
7	SF	Degumming, Braiding, Rolling, Winding, Coating	Rat/abdominal aorta	1.5 mm	Good attachment and proliferation of cells/ No functional analysis and systemic heparin administration	19
8	SF/PTFE	Degumming, dipping	Rat/abdominal aorta	1.5 mm	Gradually degrade/No functional analysis and systemic heparin administration	20
9	SF	Electrospinning	No	3 mm	Enhancement of tissue formation, extracellular matrix production, cell alignment/No animal study	46
10	PLA/PCL/ PLA:CL(50:50)	Electrospinning	No	4 mm	Contact guidance for endothelial cell growth/ No animal study	47
11	Silk fibroin/PCL	Electrospinning	Rat/carotid artery	1.5 mm	Excellent physical and functional properties without systemic anti-coagulant therapy/ small sample size in animal study	This work

[a]SF: Silk Fibroin, G: Gelatin, PET: Polyethylene terephthalate, P(LLA-CL): Poly(L-lactic acid-*co*-ε-caprolactone), PLA: Polylactic acid, PCL: Polycarprolactone, ELAS: Elastin, PLGA: Poly(lactic-*co*-glycolic acid), SF-H1: Silk fibroin with 1% heparin, SF-H2: Silk fibroin with 3% heparin, SMCs: Smooth muscle cells, ECs: Endothelial cells, BMDRMSC: Bone-marrow-derived rat mesenchymal stem cell, PTFE: Polytetrafluoroethylene, HCASMCs: Human coronary artery smooth muscle cells, HUVECs: Human umbilical vein endothelial cells, GFP-HUVECs: GFP-expressing line of HUVECs, hSMCs: Human smooth muscle cells, HAFDSC: Human amniotic fluid-derived stem cell, HAECs: Human aortic endothelial cells, NS: Not specified.

of artificial vessels may be composed of an SF scaffold with SP extract. Fibroblasts are primarily found in the outer layer of natural vessels, and therefore, the outer layer should be composed of the PCL scaffold. The results of the cellular attachment assay also revealed similar results for the MTT assay. When cells find a compatible surface, the cells spread on the surface and flatten.[43] The flattened HUVEC cells were observed on the SF scaffold with or without SP extract from day 1. However, the fibroblasts were well spread on the PCL surface.

For implantation of artificial vessels, tubular scaffolds with (*in vitro* tissue engineering) or without (non-cell seeded graft) autologous endothelial cells may be used. *In vitro* tissue engineering is expensive and time-consuming. Additionally, endothelial cells do not grow well into the lumen of small diameter tubular scaffolds. The rapid flow in the artery may detach the cultured endothelial cells, and the raw surface of the scaffold will be exposed to the blood, which can lead to thrombosis.[44]

Angiography and Color Doppler Sonography. In angiography, the vessel diameter is maintained and the function of the whole carotid vessel is maintained well without constriction (Figure 9(a)). There was no sign of obstruction or thrombosis of the reconstructive vessels. The diameter of the grafted artificial vessel was similar with the opposite carotid artery. It indicated that the normal vascular functions of the grafted artificial vessels were in order.

Using color Doppler sonography, we confirmed the vascular patency 3 weeks after operation (Figure 9). We also checked EDV, the PSV, the PI, and the RI for evaluating vascular function. The character of the implanted graft Doppler velocity waveform is shown in Figure 9(b). There was no acute thrombosis, and blood hemo-dynamics were maintained within normal function in the grafted artificial vessels.

We compared our work to selected previous works related to small diameter artificial vessels (Table III). Many previous works did not perform functional analyses, such as Doppler sonography or angiography, during follow-up, and the recipient

vessel of the animal experiment was the aorta which is not a small vessel. The results of the present study are promising and very encouraging. Thus, more animal trials should be included in future studies. Systemic administration of anti-thrombic agents may increase the success rate of the artificial vessels. In previous research, systemic administration of heparin before operation induced high success rates after grafting silk-based artificial vessels.[16] In this experiment, we did not administer any anti-thrombic agent to the animals before or after operation to evaluate the anti-thrombic effects of the SP extract in the artificial vessels. In this study, the artificial vessel in one animal failed due to thrombosis. Systemic administration of an anti-thrombic agent may be considered in future large animal studies to improve the success rate.

Histological Analysis. Fibroblast and endothelial cells were observed on the grafted artificial vessels through H&E staining (Figure 10). There were no constrictions, inflammation or blood clot formations, and neo-intimal hyperplasia was not identified.

Under inimmunohistochemical staining, the stratified cells lined with lumen were strongly positive for the antibody of von Willebrand factor (Figure 10(b)). As the von Willebrand factor is a marker of endothelial cell, the presence of newly generated endothelial cells was demonstrated. The luminal surface was fully lined with endothelial cells. In the middle layer, regenerated collagen fibers were observed using special stain (data not shown). Additionally, many fibroblasts were observed on the middle and outer layers (Figure 10).

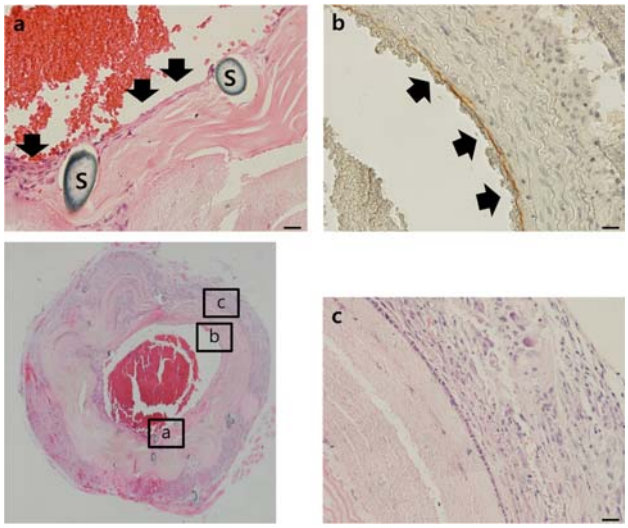

Figure 10. The cross cut of the vessel regenerated from collagen fiber (H&E stain, original magnification ×40). (a) The inner layer of the scaffold is lined with endothelial cells (arrows, bar=20 μm). The nylon sutures (S) were identified. (b) The endothelial cells in the luminal area (arrows)show strong positive to von Willebrand factor (counterstained by Mayer hematoxylin, bar=20 μm). (c) The magnified view near outer layer show many fibroblasts and a few inflammatory cells (bar=20 μm).

Conclusions

The tri-layered tubular SF and PCL nano-fiber scaffold was fabricated. The blended nano-fiber was present in the middle layer. The *in vitro* and *in vivo* results based on the vascular tube structure, the mechanical properties and the cytocompatibility of the artificial vessel indicate that this tri-layered vascular graft can potentially be used after proper preclinical investigations, and additional improvements can be made in future investigation for vascular tissue engineering.

Acknowledgments. This work was supported by a grant from the Next-Generation BioGreen21 Program (Center for Nutraceutical & Pharmaceutical Materials no. PJ01121404), Rural Development Administration, Republic of Korea. This work was supported by 'Technology Development of Marine Industrial Biomaterials' of the Marine Biotechnology Program funded by the Ministry of Oceans and Fisheries, Korea.

Supporting Information: Information is available regarding the morphologies, the average diameters, the FTIR spectrum, the DSC thermal analysis results, the contact angle, and the mechanical properties of each matrix. The materials are available *via* the Internet at http://www.springer.com/13233.

References

(1) B. Marelli, A. Alessandrino, S. Farè, G. Freddi, D. Mantovani, and M. C. Tanzi, *Acta Biomater.*, **6**, 4019 (2010).
(2) H. Bergmeister, C. Schreiber, C. Grasl, I. Walter, R. Plasenzotti, M. Stoiber, D. Bernhard, and H. Schima, *Acta Biomater.*, **9**, 6032 (2013).
(3) J. van der Slegt, S. L. Steunenberg, J. M. Donker, E. J. Veen, G. H. Ho, H. G. de Groot, and L. van der Laan, *J. Vasc. Surg.*, **1**, 120 (2014).
(4) S. L. Dahl, A. P. Kypson, J. H. Lawson, J. L. Blum, J. T. Strader, Y. Li, R. J. Manson, W. E. Tente, L. DiBernardo, M. T. Hensley, R. Carter, T. P. Williams, H. L. Prichard, M. S. Dey, K. G. Bequlman, and L. E. Niclason, *Sci. Transl. Med.*, **3**, 68 (2011).
(5) P. Lamm, G. Juchem, S. Milz, M. Schuffenhauer, and B. Reichart, *Circulation*. **104**, I108 (2001).
(6) J. A. G. Rhodin, in *Architecture of the Vessel Wall*, *Comprehensive Physiology*, John Wiley and Sons, Michigan, 2011, pp 10-31.
(7) C. Huang, S. Wang, L. Qiu, Q. Ke, W. Zhai, and X. Mo, *ACS Appl. Mater. Interfaces*, **5**, 2220 (2013).
(8) S. J. Lee, J. Liu, S. H. Oh, S. Soker, A. Atala, and J. J. Yoo, *Biomaterials*, **29**, 2891(2008).
(9) C. E. Ghezzi, B. Marelli, N. Muja, and S. N. Nazhat, *Acta Biomater.*, **8**, 1813 (2012).
(10) C. Vaz, S. Van Tuijl, C. Bouten, and F. Baaijens, *Acta Biomater.*, **1**, 575 (2005).
(11) F. G. Omenetto and D. L. Kaplan, *Science*, **329**, 528 (2010).
(12) S. C. Kundu, B. C. Dash, R. Dash, and D. L. Kaplan, *Prog. Polym. Sci.*, **33**, 998 (2008).

(13) S. C. Kundu, B. Kundu, S. Talukdar, S. Bano, S. Nayak, J. Kundu, B. B. Mandal, N. Bhardwaj, M. Botlagunta, B. C. Dash, C. Acharya, and A. K. Ghosh, *Biopolymers*, **97**, 455 (2012).
(14) B. Kundu, R. Rajkhowa, S. C. Kundu, and X. Wang, *Adv. Drug Deliv. Rev.,* **65**, 457 (2013).
(15) C. Vepari and D. L. Kaplan, *Prog. Polym. Sci*., **32**, 991 (2007).
(16) T. Fukayama, K. Takagi, R. Tanaka, Y. Hatakeyama, D. Aytemiz, Y. Suzuki, and T. Asakura, *Ann. Vasc. Surg*., **29**, 341 (2015).
(17) T. Yagi, M. Sato, Y. Nakazawa, K. Tanaka, M. Sata, K. Itoh, Y. Takagi, and T. Asakura, *J. Artif. Organs.,* **14**, 89 (2011).
(18) M. Lovett, G. Eng, J. A. Kluge, C. Cannizzaro, G. Vunjak-Novakovic, and D. L. Kaplan, *Organogenesis*, **6**, 217 (2010).
(19) Y. Nakazawa, M. Sato, R. Takahashi, D. Aytemiz, C. Takabayashi, T. Tamura, S. Enomoto, M. Sata, and T. Asakura*, J. Biomater. Sci. Polym. Ed.*, **22**, 195 (2011).
(20) S. Enomoto, M. Sumi, K. Kajimoto, Y. Nakazawa, R. Takahashi, C. Takabayashi, T. Asakura, and M. Sata, *J. Vasc. Surg*., **51**, 155 (2010).
(21) A. J. Melchiorri, N. Hibino, and J. P. Fisher, *Tissue Eng. Part B: Rev*., **19**, 292 (2013).
(22) H. Maidoub, M. Ben Mansour, F. Chaubet, M. S. Roudesli, and R. M. Maaroufi, *Biochim. Biophys. Acta*, **1790**, 1377 (2009).
(23) M. H. Son, K. H. Park, A. R. Choi, G. J. Yoo, M. J. In, D. H. Kim, and H. J. Chae, *J. Kor. Soc. Food Sci. Nutr.,* **38**, 136 (2009).
(24) B. G. Cha, H. W. Kwak, A. R. Park, S. H. Kim, S. Y. Park, H. J. Kim, I. S. Kim, K. H. Lee, and Y. H. Park, *Biopolymers*, **101**, 307 (2014).
(25) W. L. Chu, Y. W. Lim, A. K. Radhakrishnan, P. E. Lim, *BMC Complement. Altern. Med.*, **21**, 53 (2010).
(26) C. J. Bang, A. Berstad, and I. Talstad*, Haemostasis*, **21**, 155 (1991).
(27) F. Han, X. Jia, D. Dai, X. Yang, J. Zhao, Y. Zhao, Y. Fan, and X. Yuan, *Biomaterials*, **34**, 7302 (2013).
(28) A. Nieponice, L. Soletti, J. Guan, B. M. Deasy, J. Huard, W. R. Wagner, and D. A. Vorp, *Biomaterials*, **29**, 825 (2008).
(29) B. G. Cha, H. W. Kwak, A. R. Park, S. H. Kim, S. Y. Park, H. J. Kim, I. S. Kim, K. H. Lee, and Y. H. Park, *Biopolymers*, **101**, 307 (2014).
(30) H. Doshi, A. Ray, and I. L. Kothari, *Curr. Microbiol*., **54**, 213 (2007).
(31) K. Pugazhendy, *Int. J. Pharm. Biol. Arch*., **3**, 969 (2012).
(32) T. Elzein, M. Nasser-Eddine, C. Delaite, S. Bistac, and P. Dumas, *J. Colloid Interface Sci.*, **273**, 381 (2004).
(33) W. Zhou, J. He, S. Du, S. Cui, and W. Gao, *Iran. Polym. J.,* **20**, 389 (2011).
(34) M. Zoccola, A. Aluigi, C. Vineis, C. Tonin, F. Ferrero, and M. G. Piacentino, *Biomacromolecules*, **9**, 2819 (2008).
(35) Y. Nakazawa, M. Sato, R. Takahashi, D. Aytemiz, C. Takabayashi, T. Tamura, S. Enomoto, M. Sata, and T. Asakura, *J. Biomater. Sci. Polym. Ed.,* **22**, 195 (2011).
(36) K. Billiar, J. Murray, D. Laude, G. Abraham, and N. Bachrach, *J Biomed. Mater. Res*., **56**, 101 (2001).
(37) G. Konig, T.N. Mcallister, N. Dusserre, S.A. Garrido, C. Iyican, A. Marini, A. Fiorillo, H. Avila, W. Wystrychowski, K. Zagalski, M. Maruszewski, A. L. Jones, L. Cierpka, L. M. de la Fuente, and N. L'Heureux. *Biomaterials*, **30**, 1542 (2009).
(38) S. Sarkar, H. Salacinski, G. Hamilton, and A. Seifalian, *Eur. J. Vasc. Endovasc. Surg.,* **31**, 627 (2006).
(39) J. P. Stegemann, S. N. Kaszuba, and S. L. Rowe, *Tissue Eng.*, **13**, 2601 (2007).
(40) K. Kottke-Marchant, A. A. Veenstra, and R. E. Marchant, *J. Biomed. Mater. Res.*, **30**, 209 (1996).
(41) Ash. Asran, K. Razghandi, N. Aggarwal, G. H. Michler, and T. Groth, *Biomacromolecules*, **11**, 3413 (2010).
(42) G. Altankov, K. Richau, and T. Groth, *Materwiss. Werksttech*., **34**, 1120 (2003).
(43) J. E. Murphy-Ullrich, *J Clin Invest*. **107**, 785 (2001).
(44) S. Liu, C. Dong, G. Lu, Q. Lu, Z. Li, D. L. Kaplan, and H. Zhu, *Acta Biomater.*, **9**, 8991 (2013).
(45) B. Marelli, M. Achilli, A. Alessandrino, G. Freddi, M. C. Tanzi, S. Farè, and D. Mantovani, *Macromol. Biosci.*, **12**, 1566 (2012).
(46) H. Liu, X. Li, X. Niu, G. Zhou, P. Li, and Y. Fan. *Biomacromolecules*, **12**, 2914 (2011).
(47) X. Zhang, X. Wang, V. Keshav, X. Wang, J. T. Johanas, G. G. Leisk, and D. L. Kaplan, *Biomaterials*, **30**, 3213 (2009).